Dalton Transactions

Accepted Manuscript

ROYAL SOCIETY OF CHEMISTRY

www.rsc.org/dalton

Intracellular detection of Cu^{2+} and S^{2-} ions through a quinazoline functionalized benzimidazole-based new fluorogenic differential chemosensor

Anup Paul,[a*] Sellamuthu Anbu,[a] Gunjan Sharma,[b] Maxim L. Kuznetsov,[a] M. Fátima C. Guedes da Silva,[a] Biplob Koch,[b] Armando J. L. Pombeiro[a]*

[a]*Centro de Química Estrutural, Complexo I, Instituto Superior Técnico,Universidade de Lisboa, Av. Rovisco Pais, 1049-001 Lisboa. Portugal. E-mail: kanupual@gmail.com, pombeiro@tecnico.ulisboa.pt*

[b]*Department of Zoology, Faculty of Science, Banaras Hindu University, Varanasi - 221 005 (U.P.) India.*

Abstract

A new quinazoline functionalized benzimidazole-based fluorogenic chemosensor **H_3L** is synthesized and fully characterized by conventional techniques including single crystal X-ray analysis. It acts as a highly selective colorimetric and fluorescence sensor for Cu^{2+} ions in DMF/0.02 M HEPES (1:1, v/v, pH = 7.4) medium. Reaction of **H_3L** with $CuCl_2$ forms the mononuclear copper(II) $[Cu(Cl)(H_2L)(H_2O)]$ (**H_2L-Cu^{2+}**) complex which is characterized by conventional techniques and quantum chemical calculations. Electronic absorption and fluorescence titration studies of **H_3L** with different metal cations show a distinctive recognition only towards Cu^{2+} ions even in the presence of other commonly coexisting ions such as Li^+, Na^+, K^+, Mg^{2+}, Ca^{2+}, Fe^{2+}, Fe^{3+}, Mn^{2+}, Co^{2+}, Ni^{2+}, Zn^{2+}, Cd^{2+} and Hg^{2+}. Moreover, **H_2L-Cu^{2+}** acts as a metal based highly selective and sensitive chemosensor for S^{2-} ion even in the presence of other commonly coexisting anions such as F^-, Cl^-, Br^-, I^-, SO_4^{2-}, SCN^-, AcO^-, $H_2PO_4^-$, PO_4^{3-}, NO_3^-, ClO_4^-, NO_2^-, HSO_4^-, HSO_4^{2-}, $S_2O_3^{2-}$, $S_2O_8^{2-}$, CN^-, CO_3^{2-} and HCO_3^- in DMF/0.02 M HEPES (1:1, v/v, pH = 7.4) medium. Quantification analysis indicates that these receptors, **H_3L** and **H_2L-**

Cu^{2+}, can detect the presence of Cu^{2+} and S^{2-} ions at very low concentrations of 1.6×10^{-9} M and 5.2×10^{-6} M, respectively. The propensity of **H_3L** as a bio-imaging fluorescent probe to detect Cu^{2+} ions and sequential detection of S^{2-} ions by **H_2L-Cu^{2+}** in Dalton lymphoma (DL) cancer cells is also shown.

Introduction

Designing and development of selective and sensitive chemosensors for the detection of metal ions and anions is an area of growing interest owing to its important role in a wide range of environmental, clinical, chemical and biological applications.[1-5] Among the various metal cations present in the human body, Cu^{2+} is the third most abundant transition one and plays an important role in fundamental physiological processes. In addition, copper dependent enzymes can also act as catalysts to help a number of body functions to provide energy for biochemical reactions, transform melanin for pigmentation of the skin, assist the formation of crosslinks in collagen and elastin, and thereby maintain and repair connective tissues.[6-8] However, at higher concentration, it can damage the central nervous system, affect blood composition, kidneys, liver, lungs and other vital parts of the human body.[9] Owing to its significant role in various biological processes, the search for a selective fluorescence chemosensor for rapid detection of Cu^{2+} ions has become an increasingly demanding area of research.[10,11]

On the other hand, sulfide anion, a toxic, hazardous and traditional pollutant, is widely spread in the environment.[12] Hydrogen sulfide has also been found endogenously produced in endothelium cells and plays important roles in biological systems.[13] However, exposure to a high level of sulfide can lead to various physiological and biochemical problems.[14] Sulfide ion becomes even

more toxic once it gets protonated to produce HS^- or H_2S. Therefore, its detection and determination have become very important from industrial, environmental and biological points of view, and a great effort has been given to the development of suitable analytical techniques.[15] Among the conventional methods, chemosensors that rely on fluorescence or colorimetric responses can provide the most simple, inexpensive and rapid method to detect sulfide. Therefore, strategies to the design and development of these chemosensor systems have attracted a significant attention.[16] But such a type of approach has largely been devoted towards the development of cations targeting chemosensors and their bioimaging studies in living cells.[4,5] On the contrary, only a limited number of systems has been devised for bioimaging studies of fluorescent chemosensors for anions or sulfide anion detection,[17] presumably due to strong hydration which weakens the interactions of the chemosensors with the target anions.[18]

This drawback can however be overcome by using a metal displacement approach, which is of great interest and based on the larger stability constant of a metal-anion complex than that of a complex of a metal and its chemosensor.[19] Sulfide is known to react with copper ion to form very stable CuS with a very low solubility product constant $K_{sp} = 6.3 \times 10^{-36}$ (for cyanide $K_{sp} = 3.2 \times 10^{-20}$).[20] Thus, the utilization of the higher affinity of Cu^{2+} towards sulfide for designing a metal based S^{2-} fluorescence chemosensor has received considerable attention because these chemosensors show a greater S^{2-} binding affinity than organic receptors.[21]

Thus, in view of the importance of both Cu^{2+} and S^{2-} ions and taking also in consideration that no benzimidazole-based chemosensor for S^{2-} detection has been previously exploited in live cell imaging studies, we present herein a highly selective and sensitive benzimidazole-based chemosensor **H_3L** for the rapid detection of Cu^{2+} and sequential recognition of S^{2-} by the derived

complex [Cu(Cl)(H_2L)(H_2O)] (**H_2L-Cu^{2+}**), towards their application in bioimaging studies in aqueous medium.

Experimental Section

Materials and Physical Measurements

Solvents were dried and distilled prior to their use following standard procedures.[22] Reagent grade chemicals were used throughout and HPLC grade solvents were employed for spectroscopic studies. 2-(2-aminophenyl)-1-*H*-benzimidazole, 2,3-dihydroxybenzaldehyde, all the metal salts (98.0% purity) and $CuCl_2$. $2H_2O$ were purchased from Sigma Aldrich Chemical Co. and used as received. IR spectra were recorded on a Bruker Alpha Fourier transform infrared (FT-IR) spectrometer. ^{1}H (300 MHz) and ^{13}C (75.45 MHz) NMR spectra were obtained at room temperature (RT) on a Bruker 300 MHz spectrometer using tetramethylsilane [$Si(CH_3)_4$] as an internal reference. Emission spectra at room temperature were recorded on a PerkinElmer Fluorescence Spectrometer (LS-55) in DMF/0.02 M HEPES (1:1, v/v, pH = 7.4) medium. Electrospray ionization mass spectrometric data (ESI-MS) were acquired in methanol on a Bruker Micro TOF QII, and THERMO Finningan LCQ Advantage Max ion trap Mass Spectrometer.

Synthesis of 3-(5,6-dihydrobenzoimidazo-1,2-quinazolin-6-yl)benzene-1,2-diol (H_3L)

2-(2-aminophenyl)-1H-benzimidazole (0.418 g, 2.0 mmol) dissolved in ethanol (50 mL) was added to the ethanolic solution (10 ml) of 2,3-dihydroxybenzaldehyde (0.276 g, 2.0 mmol) and the resulting mixture was refluxed for 5 h. An off-white residue was isolated by removal of solvent at reduced pressure and washed several times with hexane and dried in vacuum. Pale

brown crystals suitable for X-ray analysis were obtained after two weeks by slow evaporation of N,N-dimethylformamide (DMF)/water solution. Isolated yield = 0.55 g (80%). Anal. Calcd for $C_{20}H_{15}N_3O_2$: C, 72.94; H, 4.59; N, 12.76; Found C, 73.25; H, 4.85; N, 12.89. IR (KBr pellets, cm^{-1}): 3378 (ν_{str}O–H), 3257 (ν_{str}N-H). ^{1}H NMR (DMSO-d_6, 300 MHz, δ_H, ppm): 9.64 (s, 1H, H_b), 9.09 (s, 1H, H_a), 7.96 (d, 1H, J = 7.5 Hz, H-1), 7.64 (d, 1H, J = 7.8 Hz, H-4), 7.24 (s, 1H, H-9), 7.19 (d, J = 9 Hz, 1H, H-8), 7.10 (t, 2H, H-6 and H-7), 7.06 (s, 1H, H-10), 6.86 (d, J = 9 Hz, 1H, H-5), 6.80 (t, 2H, H-2 and H-3), 6.70 (d, J = 9 Hz, 1H, H-11), 6.45(t, 1H, H-12), 6.19 (d, J = 9 Hz, 1H, H-5). ^{13}C NMR (DMSO-d_6, 75.45 MHz, δ_C, ppm): 147.6, 145.9, 144.4, 143.9, 142.9, 133.4, 131.9, 127.5, 125.0, 122.6, 122.4, 119.7, 119.0, 118.2, 116.8, 115.9, 115.2, 111.9, 110.7, 63.2. ESI-MS in CH_3OH *m/z* 330.10 (Calcd. 330.12) for [**H_3L** + H]$^+$and 352.11 (cacld.352.35) for [**H_3L** + Na]$^+$. UV/vis-$\lambda_{max,}$ nm (ε, $M^{-1}cm^{-1}$) in DMF/0.02 M HEPES (1:1, v/v, pH = 7.4): 338 (1.24×10^4) and 274 (1.77×10^4).

Synthesis of the monocopper(II) complex [H_2L-Cu^{2+}]

An aqueous solution of $CuCl_2.2H_2O$ (0.170 g, 1.0 mmol) was added dropwise to an ethanolic suspension of **H_3L** (0.329 g, 1.0 mmol) with constant stirring. The reaction mixture turned dark brown immediately and was stirred for 2 h at room temperature. The resulting solution was filtered and kept for crystallization. Brownish crystalline materials were deposited after a couple of days. Yield: 0.249 g (50%). Anal. Calcd for $C_{20}H_{16}ClCuN_3O_3$: C, 53.94; H, 3.62; N, 9.44; Found C, 54.10; H, 3.81; N, 9.58. IR (KBr pellets, cm^{-1}): 3422 (ν_{str}O–H). ESI-MS in CH_3OH *m/z* 391.00 (Calcd. 391.04) for $[Cu(H_2L)]^+$. UV/vis–$\lambda_{max,}$ nm (ε, $M^{-1}cm^{-1}$) in DMF/0.02 M HEPES (1:1, v/v, pH = 7.4): 392 (1.09×10^4) and 281 (3.16×10^4).

Sensor Studies

Stock solutions of the **H_3L** and **H_2L-Cu^{2+}** for electronic absorption and fluorescence (5 μM) titration studies were prepared in DMF/0.02 M HEPES (1:1, v/v, pH = 7.4) medium. The solution of respective metal ions (Li, Na^+, K^+, Mg^{2+}, Ca^{2+}, Mn^{2+}, Co^{2+}, Ni^{2+}, Cu^{2+}, Fe^{2+}, Zn^{2+}, Cd^{2+}, Cu^{2+} and Hg^{2+}) were prepared by dissolving their chloride salts in triple distilled water (1 mM). In a typical titration, the solution of **H_3L** and **H_2L-Cu^{2+}** were taken in a quartz cuvette (3.0 mL; path length, 1 cm) and diluted stock solution of the metal ions were added gradually with the help of a micropipette. The spectral changes for **H_3L** and **H_2L-Cu^{2+}** were recorded as a function of metal ions added and all experiments were repeated thrice.

Crystal Structure Determination

Suitable crystal for single crystal X-ray analyses of **H_3L** was obtained from slow evaporation of DMF (N,N-dimethylformide)/water. The crystal was mounted in a nylon loop and measured at 296 K. Intensity data were collected using a Bruker APEX-II PHOTON 100 diffractometer with graphite monochromated Mo Kα (λ = 0.71069 nm) radiation. Data were collected using phi and omega scans of 0.5° per frame and a full sphere of data was obtained. Cell parameters were retrieved using Bruker SMART[23a] software and refined using Bruker SAINT[23a] on all the observed reflections. Absorption corrections were applied using SADABS.[23a] Structure was solved by direct methods by using the SHELXS-97 package[23b] and refined with SHELXL-2013.[23b] Calculations were performed using the WinGX System-Version 1.80.03.[23c] All non-hydrogen atoms were refined anisotropically. The hydrogen atoms bonded to carbon were included in the model at geometrically calculated positions and refined using a riding model. The hydrogen atoms bound to O- and N-atoms were located in the difference Fourier synthesis and refined with the help of distance restraints. During the refinement of the structure, electron

density peaks were located and believed to be two highly disordered DMF molecules (by counting the number of electrons suppressed). All the attempts made to model these solvent molecules were not successful and they were removed using the SQUEEZE routine from PLATON.[23d] The reported final sum formula contains all atoms that are most possibly present in the crystal and thus contributed to the scattering.

Computational Details

The full geometry optimization of the copper complexes has been carried out at the DFT level of theory using the M06-2X functional with the help of the Gaussian-09 program package.[24] The relativistic Stuttgart pseudopotential that described 10 core electrons (MDF10) and the appropriate contracted basis set were employed for the Cu atom while the standard basis set 6-31G* was applied for all other atoms.[25] The single-point calculations were then performed with the 6-311+G** basis set for all non-metal atoms. No symmetry operations have been applied for any of the structures calculated. The Hessian matrix was calculated analytically for the optimized structures in order to prove the location of correct minima (no imaginary frequencies) and to estimate the thermodynamic parameters, the latter being calculated at 25 °C.

Total energies corrected for solvent effects (E_s) were estimated at the single-point calculations on the basis of gas-phase geometries using the polarizable continuum model in the CPCM version with water taken as solvent.[26] The UAKS model was applied for the molecular cavity and dispersion, repulsion and cavitation terms were taken into account. The entropic term for the water solvent (S_s) was calculated according to the procedure described by Wertz and Cooper and Ziegler using equation:[27, 28]

$$S_s = S_g + [(-14.3 \text{ cal/mol•K}) - 0.46(S_g - 14.3 \text{ cal/mol•K}) + 7.98 \text{ cal/mol•K}]$$

Where S_g is the gas-phase entropy of solute. The enthalpies and Gibbs free energies in solution (H_s and G_s) were estimated using the expressions:

$$H_s = E_s(6\text{-}311+G^{**}) - E_g(6\text{-}311+G^{**}) + H_g(6\text{-}31G^{*})$$

$$G_s = H_s - T•S_s$$

Where E_g and H_g are the gas-phase total energy and enthalpy calculated at the corresponding level.

Measurement of cytotoxicity by MTT assay

The MTT assay[29] has been applied to evaluate the cytotoxicity of chemosensor **H_3L** and its copper(II) complex **H_2L-Cu^{2+}** on live DL cells before fluorescence imaging. To estimate the cell viability and proliferation, Dalton's lymphoma (DL) (Murine lymphoma) cells were seeded at 2.5×10^4 cells/well in RPMI-1640 medium with 10% Fetal Bovine Serum (FBS) in 96-well plates. Seeded DL cells were treated with increasing concentrations of **H_3L** and **H_2L-Cu^{2+}** dissolved in DMSO (stock solution, 100 mM) and diluted with RPMI-1640 (the concentration of DMSO did not exceed 0.1% v/v) and incubated for 24 h. After incubation the cells were washed with PBS and MTT was added (*c*, 0.5 μg/100 μL). These were again incubated for 2 h at 37 °C and the formazan crystals formed were dissolved in DMSO. After 30 min the absorbance (at 570 nm) was measured using an ELISA plate reader. The results were expressed as percentage of the cell viability with respect to control.

Dose response curves were obtained by plotting the percent cell survival (percent control) *vs.* the drug concentration. Percent control was calculated using the following formula:

% Control = [Mean O. D. of Drug treated well/Mean O. D. of control well] × 100

Cell imaging experiment

DL (1×10^{-6}) cells were incubated with **H_3L** (5 μM) in RPMI-1640 with 10% FBS (Fetal Bovine Serum) for 1 h at 37 °C. $CuCl_2$ (5 μM) was added to the DL cells with **H_3L** for 0.5 h and further Na_2S (5 and 10 μM, respectively) was added for 0.5 h. Cells were washed with PBS and fluorescent images were captured by fluorescent microscope (Evos FL, Life technologies) in phase contrast and blue channel simultaneously.

Results and Discussion

Synthesis and Characterization

The chemosensor **H_3L** was synthesized (*ca.* 80 % yield) by condensation of 2-(2-aminophenyl)-1H-benzimidazole with 2,3-dihydroxybenzaldehyde (1:1) in ethanol and the corresponding monocopper(II) complex $[Cu(Cl)(H_2L)(H_2O)]$ (**H_2L-Cu^{2+}**) was prepared (*ca.* 50 % yield) by reacting **H_3L** with $CuCl_2.2H_2O$ in an ethanol-water binary mixture (Scheme 1).

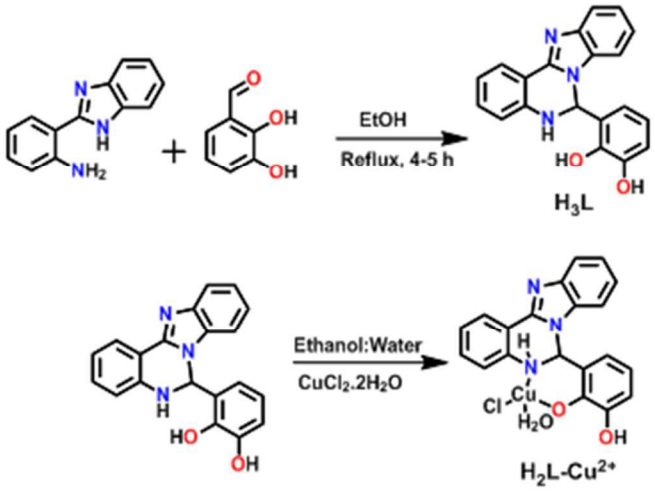

Scheme 1. Synthesis of the chemosensor **H_3L** and its copper(II) complex **H_2L-Cu^{2+}**.

Both **H_3L** and **H_2L-Cu^{2+}** were fully characterized by elemental analyses, IR, ^1H and ^{13}C (in the case of **H_3L**) NMR and ESI-MS techniques. The crystal structure of **H_3L** was further confirmed by single crystal X-ray crystallography analysis. The ^1H NMR spectrum of **H_3L** exhibits two distinct singlets due to the two phenolic (-OH) protons at δ 9.64 ($-OH_b$) and δ 9.09 ($-OH_a$), respectively (Fig. S1, ESI). The signals at δ 7.24 and 7.06 are assigned to -NH (H-9) and -CH (H-10) of the quinazoline ring (Fig. S1, ESI). The ^{13}C NMR spectrum also agrees with the formula (Fig. S2, ESI). The positive ion ESI mass spectrum of **H_3L** (Fig. S3, ESI) displays peaks at *m/z* = 330.10 (calcd. 330.12) and 352.11 (calcd. 352.35) corresponding to $[M + H]^+$ and $[M + Na]^+$, respectively. The chemosensor **H_3L** derived copper(II) complex **H_2L-Cu^{+2}** shows a major peak at *m/z* = 467.76 (calcd. 467.10), assigned to the $[Cu(Cl)(H_2L)(H_2O) + Na]^+$ species, followed by a peak at *m/z* = 391.26 (calcd. 391.04), assigned to $[Cu(H_2L)]^+$, which strongly supports the formation of the complex **H_2L-Cu^{+2}** (Fig. S4, ESI). Further, the simulated isotopic mass distribution (Fig. S5, ESI) (obtained using http://www.chemcalc.org) and observed (Fig. S5, ESI) isotopic mass distribution of **H_2L-Cu^{+2}** at *m/z* = 467.76 are in good agreement with the proposed formulation of **H_2L-Cu^{+2}**.

A crystal of **H_3L** suitable for X-ray diffraction analysis was obtained by slow evaporation from a DMF and water solution. It crystallizes in the C 2/c monoclinic system (Fig. 1), its asymmetric unit comprising one molecule of the compound and half of a molecule of water. The formation of the quinazoline skeleton is clearly evidenced. Crystallographic data and refinement parameters are summarized in Table 1 and selected bond distances and angles are presented in the legend of Fig. 1.

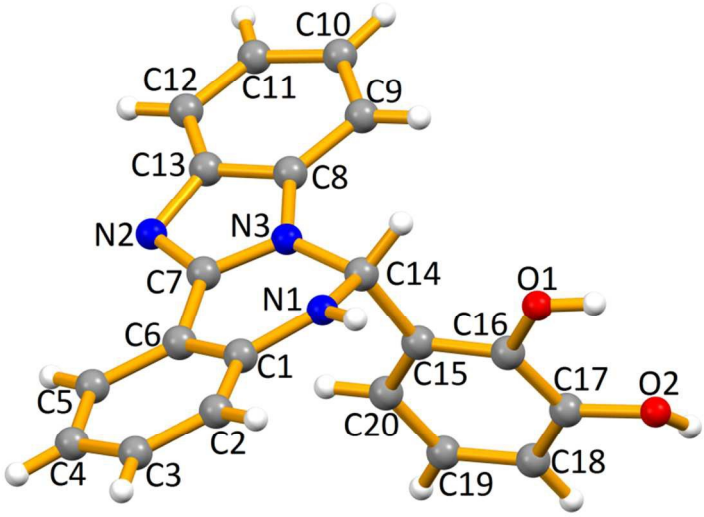

Fig. 1. Ball and stick representation of **H_3L**. The crystallization water molecule was omitted for clarity. Selected bond distances (Å) and angles (º): C14–N1 1.446(4), C14–N3 1.456(4), C14–C15 1.536(4), C16–O1 1.369(4), C17–O2 1.376(4); N1–C14–N3 106.9(3), N1–C14–C15 113.7(3), N3–C14–C15 111.7(2).

No suitable crystals for X-ray diffraction studies were obtained for the **H_2L-Cu^{2+}** complex. However, apart from the consistent elemental, IR and ESI-MS^+ data (see above), its 1:1 ligand:metal stoichiometry is confirmed by ^{1}H NMR studies, whereas the complete formula [Cu(Cl)(H_2L)(H_2O)] is established by quantum chemical calculations, as shown below.

^{1}H NMR studies

We have performed ^{1}H NMR titration studies to confirm the deprotonation of a phenolic OH group and the 1:1 stoichiometry between **H_3L** and **Cu^{2+}** ion in DMSO-d_6 (Fig. 2). Upon addition of Cu^{2+} (0.5 equiv) to a solution of **H_3L**, the resonance due to the phenolic protons -OH (H_a and H_b; δ 9.71 and 9.15) shifted marginally and appeared at δ 9.86 and 9.18, respectively. Further

additions of Cu^{2+} (~1.0 equiv.) led to complete disappearance of the phenolic -OH_a, while the signal due to the -OH_b proton shifted significantly and appeared in the downfield region at δ 10.13 (Fig. 2). The disappearance of the -OH_a proton confirms the participation of this group upon deprotonation in complex formation, which is in accord with the quantum chemical calculations (see below) of the proposed structure of **H_2L-Cu^{2+}**. Moreover, it is noteworthy to mention that a well resolved ^{1}H NMR spectrum for **H_2L-Cu^{2+}** could not be obtained due to the paramagnetic character of the Cu^{2+}(d^9) system which also accounts for the decreased spectral resolution upon addition of Cu^{2+}.[30]

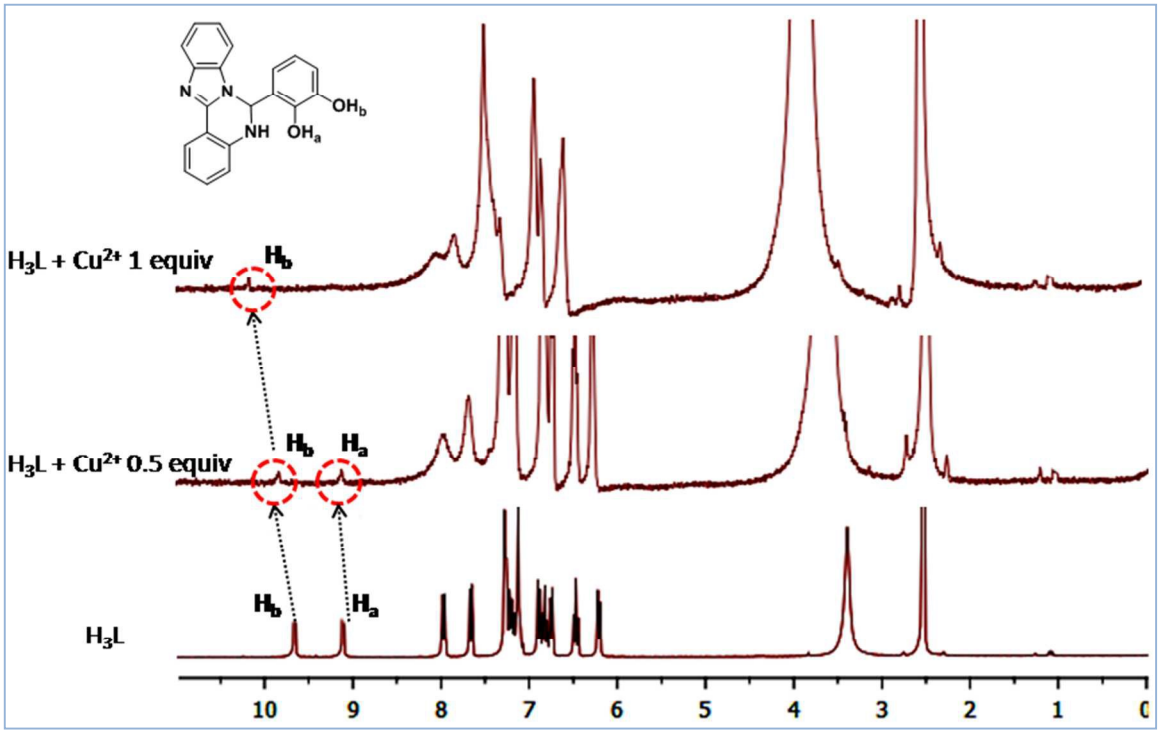

Fig. 2. ^{1}H NMR titration spectra (stacked) of **H_3L** in the presence of Cu^{2+} at room temperature in DMSO-d_6.

Quantum chemical calculations

Since, after several attempts, crystals of the copper complex **H_2L-Cu^{2+}** suitable for X-ray analysis could not be obtained, the possible structure of this species was investigated by theoretical DFT methods. Five of the most plausible structures of this complex were fully optimized (Fig. 3). In the structures **a-c** described by the general formula [Cu(Cl)(H_2L)(H_2O)], the simply deprotonated H_2L^- ligand exhibits a bidentate coordination mode, of either O,N- or O,O- type. Structure **a** with the coordinated amino N atom is significantly more stable than both **b** and **c** (by 18.4 and 11.3 kcal/mol, respectively, in terms of ΔG_s). The calculated spin density in all **a-c** structures exhibits a noticeable delocalization between the Cu ion and the donor atoms of the ligands (Fig. 4), the spin density value at the Cu atom being 0.73-0.78 e.

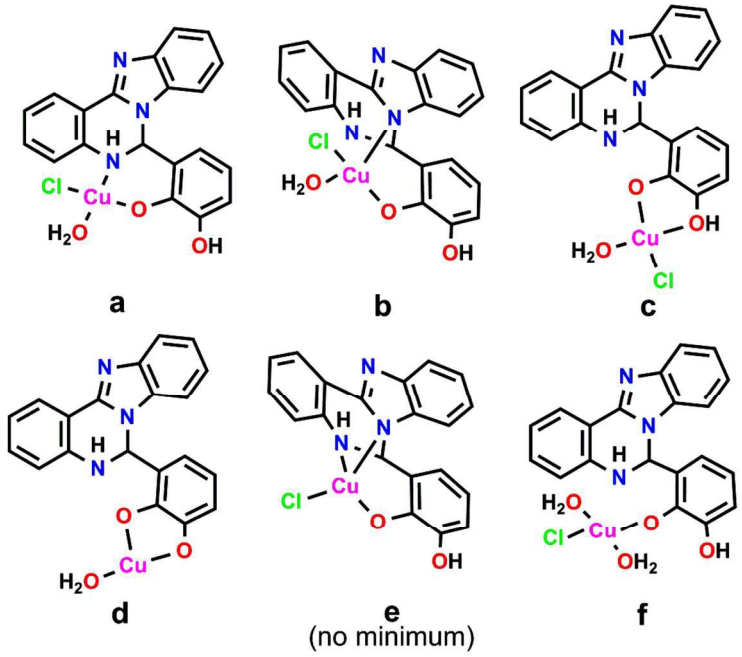

Fig. 3. Calculated structures of **H_2L-Cu^{2+}.** The most stable one is **a.**

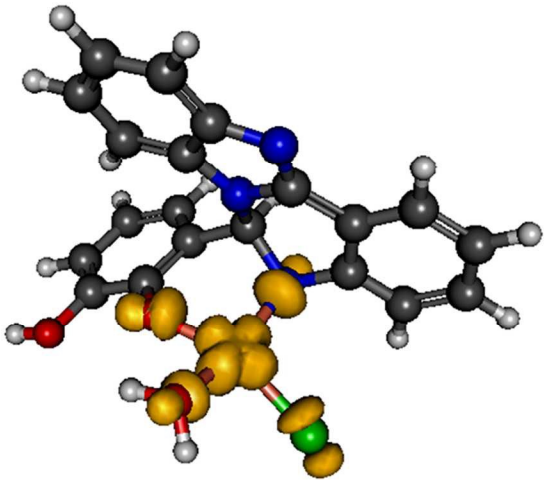

Fig. 4. Spin density distribution in complex [Cu(Cl)(H_2L)(H_2O)] (**a**).

The optimization of another bidentate structure, [Cu(HL)(H_2O)$_2$], with two O donor atoms resulted in the extrusion of one water ligand to the second coordination sphere to give complex [Cu(HL)(H_2O)](H_2O) (**d**). The calculated ΔG_s values of its formation from **a** [reaction (1)] is highly positive (37.6 kcal/mol) indicating the low thermodynamic stability of **d**. The spin density is delocalized among the oxygen and carbon atoms of the ligand HL^{2-} and it is virtually zero at Cu (Fig. S6, ESI), indicating the oxidation state +1 of the metal and a non-innocent character of HL^{2-} in this structure.

$$[Cu(Cl)(H_2L)(H_2O)]\ (\mathbf{a}) + H_2O \rightarrow [Cu(HL)(H_2O)](H_2O)\ (\mathbf{d}) + HCl \qquad (1)$$

Structure [Cu(Cl)(H_2L)] (**e**) with the tridentate ligand H_2L^- is not stable and is transformed to the **a** type structure as a result of the geometry optimization. Finally, the addition of one water molecule to the seesaw type complex **b** led to the decoordination of the nitrogen atom and formation of the square-planar species [Cu(Cl)(H_2L)(H_2O)$_2$] (**f**) with the monodentate H_2L^- (Fig.

3). The energy of structure **f** was found to be 2.4 kcal/mol higher than the sum of the energies of **a** + H_2O. Thus, the calculations indicate that the most stable coordination mode of the copper complex **H_2L-Cu^{2+}** is the bidentate one with the O and amino N donor atoms (structure **a**).

pH-dependent behaviour of H_3L and H_2L-Cu^{2+}

In order to investigate the effect of pH on the emission properties of **H_3L**, its fluorescence spectra (5 μM) in DMF/0.02 M HEPES at different pH (*ca.* 3-12) values were investigated (Fig. S7, ESI). The fluorescence spectrum of the **H_3L** (5 μM) exhibits a strong emission at λ = 425 nm (λ_{ex} = 365 nm) in DMF/0.02 M HEPES (1:1, v/v, pH = 7.4) medium. The decrease of fluorescence intensity at low pH values can be attributed to protonation of the quinazoline moiety which leads to proton-induced fluorescence quenching.[31] Under high pH conditions, the base induced deprotonation of phenolic -OH may lead to photoinduced electron transfer (PET) from the electron-rich phenol moiety to the benzimidazole fluorophore, what could account for the fluorescence quenching of **H_3L**.[31] On the other hand, the fluorescence of **H_2L-Cu^{2+}** does not vary within a very wide pH window (*ca.* 3-12) (Fig. S7, ESI). Thus, the pH of 7.4 was maintained throughout the sensor experiments.

Cation sensing studies of H_3L

The electronic absorption spectrum of **H_3L** (5 μM) exhibits three prominent bands at 356, 302 and 291 nm (ε = 1.2 × 10^4, 2.5 × 10^4 and 2.3 × 10^4 $M^{-1}cm^{-1}$, respectively) (Fig. S8, ESI). The absorption band at 356 nm has been attributed to n-π* transitions, while the others have been assigned to the π–π* transitions.[31] In order to examine the interaction of **H_3L** with various cations, a solution of **H_3L** was treated with 2 equiv. of chloride salts of Li^+, Na^+, K^+, Mg^{2+}, Ca^{2+},

Fe^{2+}, Fe^{3+}, Mn^{2+}, Co^{2+}, Ni^{2+}, Zn^{2+}, Cd^{2+}, Cu^{2+} and Hg^{2+}. No notable change was observed upon addition of any of these metal ions (Fig. 5A), with the exception of Cu^{2+} whose addition induced a significant change with appearance of new bands at 300 and 430 nm ($\varepsilon = 3.9 \times 10^4$ and 0.66×10^4 $M^{-1}cm^{-1}$, respectively). The appearance of the completely new band at 430 nm, strongly suggests the interaction of Cu^{2+} with a phenolic oxygen of **H_3L** to form the complex **H_2L-Cu^{2+}.**[32]

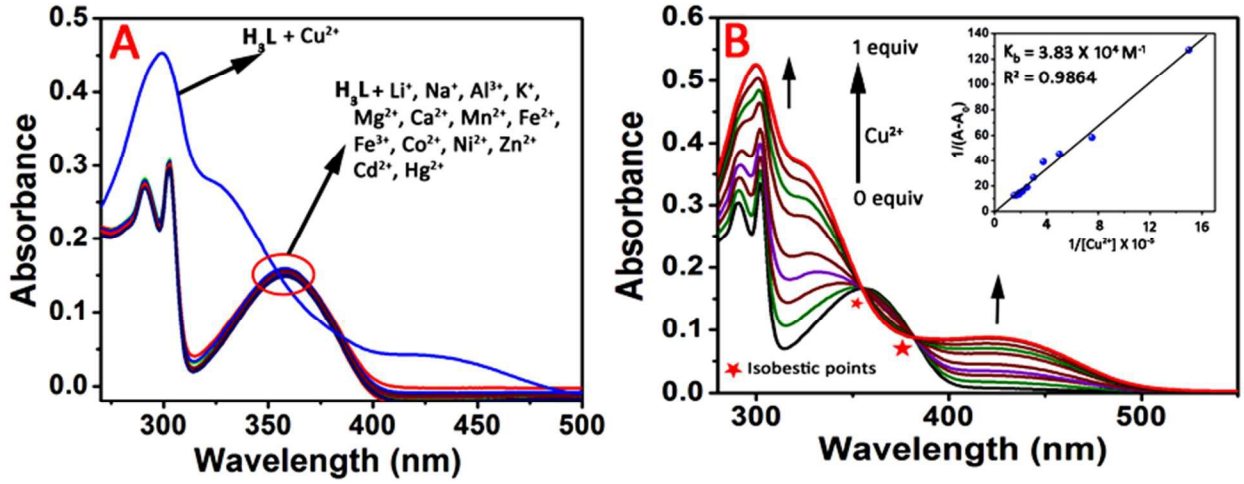

Fig. 5. (A) Change in the absorption spectrum of the receptor **H_3L** (5 μM) in the presence of various metal ions (2 equiv.) and (B) in the presence of increasing concentration (0-5 μM) of Cu^{2+} in DMF/0.02 M HEPES (1:1, v/v, pH = 7.4) (Inset shows the Benesi-Hildebrand plot).

In order to determine the binding behaviour of **H_3L** towards Cu^{2+} ion, titration experiments have been performed. Gradual addition of Cu^{2+} in increasing concentration (0-5 μM) led to the disappearance of the bands at 291 and 302 nm with the concomitant appearance of the new absorption band at 430 nm, attributed to the formation of the **H_2L-Cu^{2+}** complex. Reaction of **H_3L** with Cu^{2+} was also evidenced from the change in the color of the solution, which gradually turned from colourless to light brown (Fig. S9, ESI). Moreover, the appearance of well-defined isosbestic points at 354 and 382 nm are consistent with an equilibrium between of **H_3L** and its

copper(II) complex $\mathbf{H_2L{-}Cu^{2+}}$ in solution (Fig. 5B). The binding constant K_b was evaluated using the Benesi-Hildebrand equation ($K_b = 3.8 \times 10^4\ M^{-1}$). The Job's plot analysis at 425 nm revealed 1:1 stoichiometry for $\mathbf{H_3L}$ and $\mathbf{Cu^{2+}}$ (Fig. S10, ESI).

In order to prove the selectivity of $\mathbf{H_3L}$ towards Cu^{2+}, we carried the fluorescence experiment of $\mathbf{H_3L}$ with other alkali (Li^+, Na^+, K^+), alkali-earth (Mg^{2+}, Ca^{2+}) and 3d-series (Mn^{2+}, Fe^{2+}, Fe^{3+}, Co^{2+}, Ni^{2+}, Zn^{2+}, Cd^{2+} and Hg^{2+}) metal ions. As shown in Fig. 6A, $\mathbf{H_3L}$ is highly fluorescent at λ = 425 nm (λ_{ex} = 365 nm) and addition of only Cu^{2+} leads to a dramatic fluorescence quenching response (*ca.* 58 fold), while the other metal ions, such as Li^+, Na^+, K^+, Mg^{2+}, Ca^{2+}, Mn^{2+}, Fe^{2+}, Fe^{3+}, Co^{2+}, Ni^{2+}, Zn^{2+}, Cd^{2+} and Hg^{2+}, do not led to any significant fluorescence quenching under identical spectroscopic conditions. These observations clearly indicate the excellent selectivity of the probe $\mathbf{H_3L}$ towards only Cu^{2+}.

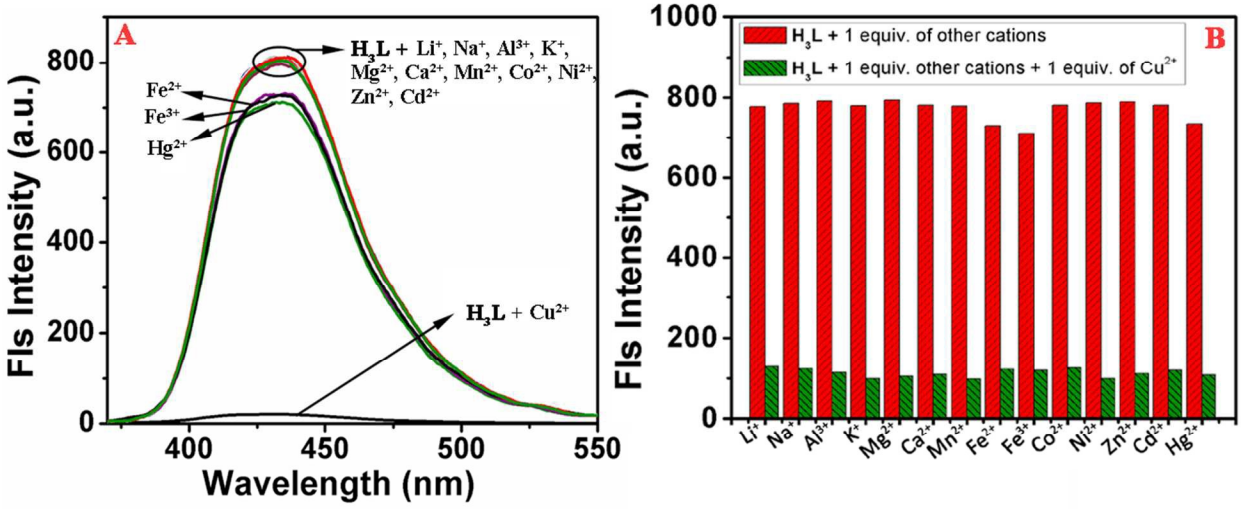

Fig. 6. (A) Change in the initial fluorescence intensity of chemosensor $\mathbf{H_3L}$ (5 μM) in presence of 1.0 equiv. of different metal cations and (B) competitive selective binding affinity of $\mathbf{H_3L}$ (5 μM) towards Cu^{2+} in the presence of 1.0 equiv. of different metal cations in DMF/0.02 M HEPES (1:1, v/v, pH = 7.4) (The intensities were recorded at λ_{em}= 425 nm at room temperature).

To substantiate the practical applicability of **H_3L** as a selective fluorescence probe for Cu^{2+} ions, we carried out a competitive fluorescence titration study with the aforesaid competing metal ions. Upon mixing with one equivalent of any other metal cation, the initial fluorescence intensity of **H_3L** did not alter significantly (red bars, Fig. 6B). However, subsequent addition of one equivalent of Cu^{2+} led to a fluorescence quenching (green bars), which further demonstrates the excellent selectivity and sensitivity of the sensor **H_3L** for Cu^{2+}ions even in the presence of other competing metal ions (Fig. 6B). To evaluate the rapid response of the probe **H_3L** towards Cu^{2+}, a time dependent fluorescence experiment of **H_3L** with excess of Cu^{2+} (*ca*. 5.0 equiv.) was conducted, and *ca.* 58 fold decrease in fluorescence intensity was observed in just *ca.* 2.5 min, subsequently reaching saturation after *ca.* 5.0 min (Fig. S11, ESI).

Fluorescence titration between **H_3L** (5 μM) and Cu^{2+} (0-1 equiv.) in DMF/0.02 M HEPES (1:1, v/v, pH = 7.4) medium was carried out. Gradual addition of Cu^{2+} (0-1 equiv.) to a solution of **H_3L** resulted in a decrease of the fluorescence intensity which quenched almost completely when 1.0 equivalent of Cu^{2+} was employed (Fig. 7). This quenching possibly could be due to the paramagnetic and incomplete d shell of the Cu^{2+} ion. That eventually makes this ion to exhibit discernible quenching of the fluorescence intensity via electron- and/or energy-transfer process in complex formation.[33] The Job's plot (Fig. S12, ESI) analysis of the fluorescence titration profile of **H_3L** (5 μM) revealed a 1:1 stoichiometry between **H_3L** and Cu^{2+} and the calculated Benesi-Hildebrand binding constant was found to be 2.6×10^4 M^{-1}. Further, the fluorescence titration profile demonstrates that **H_3L** has a detection limit of 1.62 nM (100 ppt) for Cu^{2+} (Fig. S13, ESI), which is comparable to the other reported Cu^{2+} chemosensors[34] and below the acceptable level in drinking water and the typical concentration of blood copper (15.7-23.6 M) in normal individuals as defined by the U.S. Environmental Protection Agency.[35]

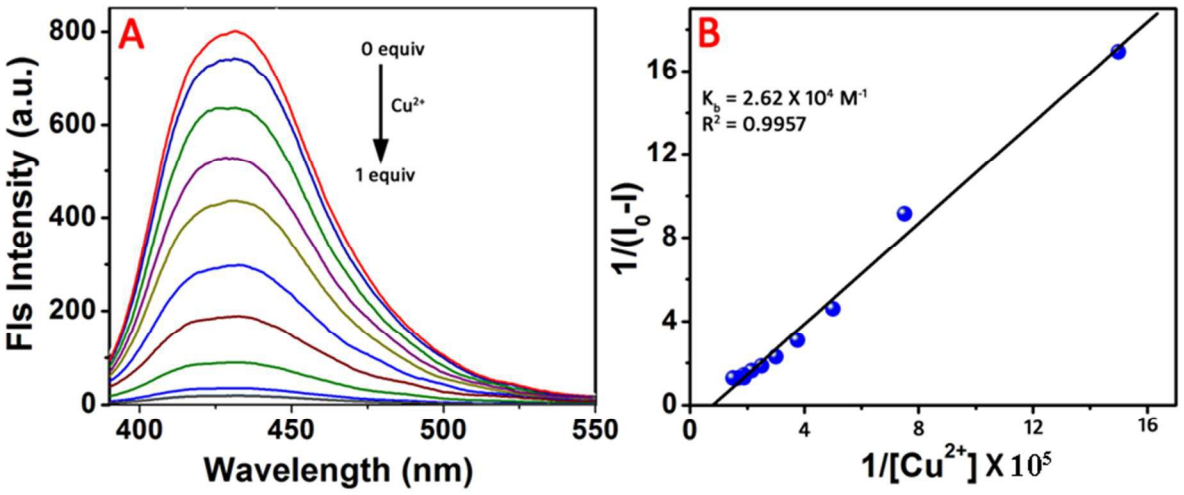

Fig. 7. (A) Change in the fluorescence spectra upon gradual increase in concentration of Cu^{2+}(0-5 μM) in DMF/0.02 M HEPES buffer (1:1, v/v, pH = 7.4) medium at λ = 425 nm (λ_{ex} = 365 nm). (B) Benesi-Hildebrand plot.

Anion sensing studies of H_2L-Cu^{2+}

In addition to the metal-ion sensing properties of **H_3L**, we have also investigated the binding behaviour of the metal based chemosensor **H_2R-Cu^{2+}** towards different anions using absorption and fluorescence spectral techniques in DMF/0.02 M HEPES buffer (1:1, v/v, pH = 7.4) medium. The electronic absorption spectrum of **H_2L-Cu^{2+}** displays two absorption bands at 300 and 430 nm (ε = 4.1 $\times 10^4$ and 0.95 $\times 10^4$ $M^{-1}cm^{-1}$, respectively) attributed to n–π* and π–π* transitions, respectively (Fig. S8, red line, ESI). Addition of an excess of F^-, Cl^-, Br^-, I^-, SO_4^{2-}, SCN^-, AcO^-, $H_2PO_4^-$, PO_4^{3-}, NO_3^-, ClO_4^-, NO_2^-, HSO_4^-, HSO_4^{2-}, $S_2O_3^{2-}$, $S_2O_8^{2-}$, CO_3^{2-} and HCO_3^- to a solution of **H_2L-Cu^{2+}** (5 μM) did not show any significant change in the absorption (Fig. S14, ESI). However, addition of S^{2-} or CN^- led to significant changes in both the absorption and emission spectra of **H_2L-Cu^{2+}**. In the absorption titration profile, gradual addition of S^{2-} (1.0 equiv.) to a solution of **H_2L-Cu^{2+}** led to a decrease in the absorption band intensity at 300 nm

accompanied by the development of two new bands at 291 and 302 ($\varepsilon = 2.1 \times 10^4$ and 2.6×10^4 $M^{-1}cm^{-1}$, respectively) (Fig. 8A), what is attributed to the regeneration of the absorption bands of **H_3L**, triggered by the decomplexation of **H_2L-Cu^{2+}**. The well-defined isobestic points centred at λ = 378 nm and 359 nm also suggest the conversion into a new chemical entity in solution. The Benesi-Hildebrand binding constant (K_b) value estimated from the absorption (Inset Fig. 8A) titration profiles is found to be 3.1×10^4 M^{-1}. An analogous spectral pattern is observed in the presence of 1.0 equiv of CN^- in the absorption titration profile between **H_2L-Cu^{2+}** and CN^- ($K_b = 2.97 \times 10^4$ M^{-1}) (Fig. S15, ESI). Furthermore, the changes observed in the absorption titration profiles between **H_2L-Cu^{2+}** and S^{2-}/CN^- are the reverse of those occurring during the titration between **H_3L** and Cu^{2+}. These results clearly demonstrate the decomplexation of **H_2L-Cu^{2+}** by the sulfide and cyanide ions, leading to the free probe **H_3L**.

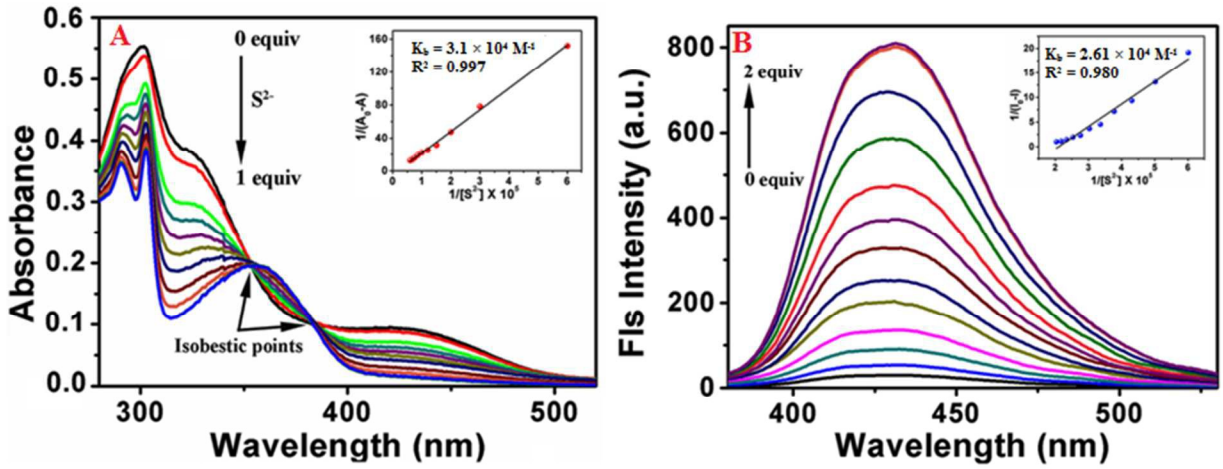

Fig. 8. Change in the absorption (A) and fluorescence (B) intensity (λ_{ex} = 365 nm) of **H_2L-Cu^{2+}** (5 μM) upon gradual addition of a S^{2-} solution in DMF/0.02 M HEPES (1:1, v/v, pH = 7.4) medium. Insets show the corresponding Benesi-Hildebrand plot (A) and titration curve of **H_2L-Cu^{2+}** *vs*. the ratio of S^{2-} and **H_2L-Cu^{2+}** concentrations (B).

In the fluorescence titration experiments, addition of S^{2-} to a $\mathbf{H_2R\text{-}Cu^{2+}}$ solution led to a significant increment in the fluorescence intensity at 425 nm and the emission reached its saturation when 2 equiv. of S^{2-} (relative to $\mathbf{H_3L}$) were added (Fig . 8B). This could be ascribed to the S^{2-} induced fluorescence enhancement, which can be accounted for by the Cu^{2+} displacement as shown in Fig. 9. In the absence of S^{2-} ions, the $\mathbf{H_2L\text{-}Cu^{2+}}$ complex shows a weak fluorescence emission, while in the presence of S^{2-}, $\mathbf{H_2L\text{-}Cu^{2+}}$ undergoes displacement with decomplexation to form free $\mathbf{H_3L}$ and CuS in the medium,[17] leading to a highly fluorescent '*switch-on*' response with only 2 equiv. of S^{2-}, due to the restoration of $\mathbf{H_3L}$ (Fig. 9). This observation is further supported by the colour change of the $\mathbf{H_2L\text{-}Cu^{2+}}$ solution from light brown to colourless (Fig. S8, ESI). A similar spectral pattern was observed upon introduction of the CN^- ion, but the emission reached its saturation only when 80 equiv. of CN^- ion (relative to $\mathbf{H_3L}$) were added (Fig. S16, ESI).

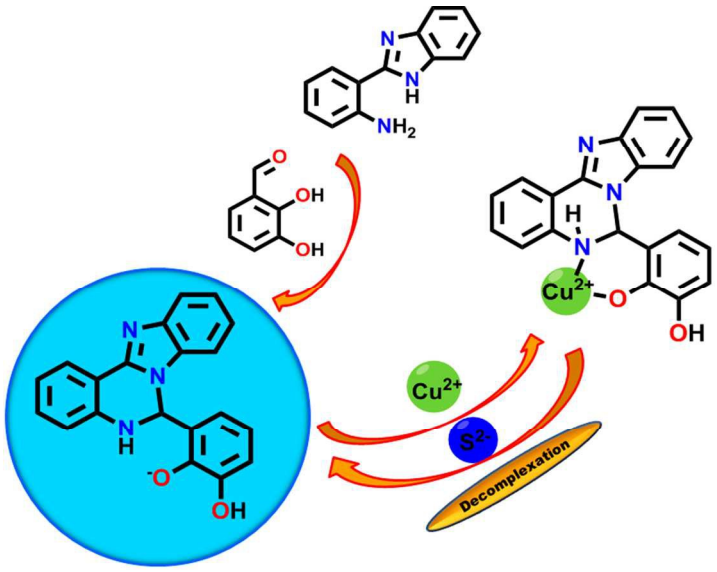

Fig. 9. Plausible mechanism for Cu^{2+} detection *via* $\mathbf{H_2L\text{-}Cu^{2+}}$ complex formation (*Turn-off*); and subsequent S^{2-} recognition leading to decomplexation and to fluorescence revival of $\mathbf{H_3L}$ (*Turn on*).

The Benesi-Hildebrand binding constant estimated from the fluorescence titration profile for S^{2-} is 2.61×10^4 M^{-1} (Fig. 8A, Inset).

Further, a competitive anion selectivity study was performed by adding S^{2-} to a solution containing **H_2L-Cu^{2+}** and a tested anion (*ca.* 10 equiv.). The fluorescence response was monitered at λ_{em} = 425 nm (λ_{ex} = 365 nm) and is presented as a bar diagram (Fig. 10). Although addition of any individual anion (10 equiv.) to **H_2L-Cu^{2+}** causes an insignificant change in the fluorescence intensity (except for CN^-), this however fully increases upon addition of S^{2-} due to the liberation of **H_3L**. These experiments clearly indicate the favourable detection of S^{2-} over the other anions.

In order to evaluate the practical utility, the detection limit of **H_2L-Cu^{2+}** for S^{2-} was also evaluated. Its value, 5.2 μM (Fig. S17, ESI), indicates that the **H_2L-Cu^{2+}** ensemble can be used as a good selective fluorescent sensor for S^{2-}. Furthermore, time dependent fluorescence experiments of **H_2L-Cu^{2+}** with an excess of S^{2-} (*ca.* 3 equiv) indicated complete resurgence in fluorescence intensity in just *ca.* 20 sec. (Fig. S18, ESI), also pointing that the complex **H_2L-Cu^{2+}** behaves as an efficient and sensitive probe towards S^{2-} ion recognition in aqueous media.

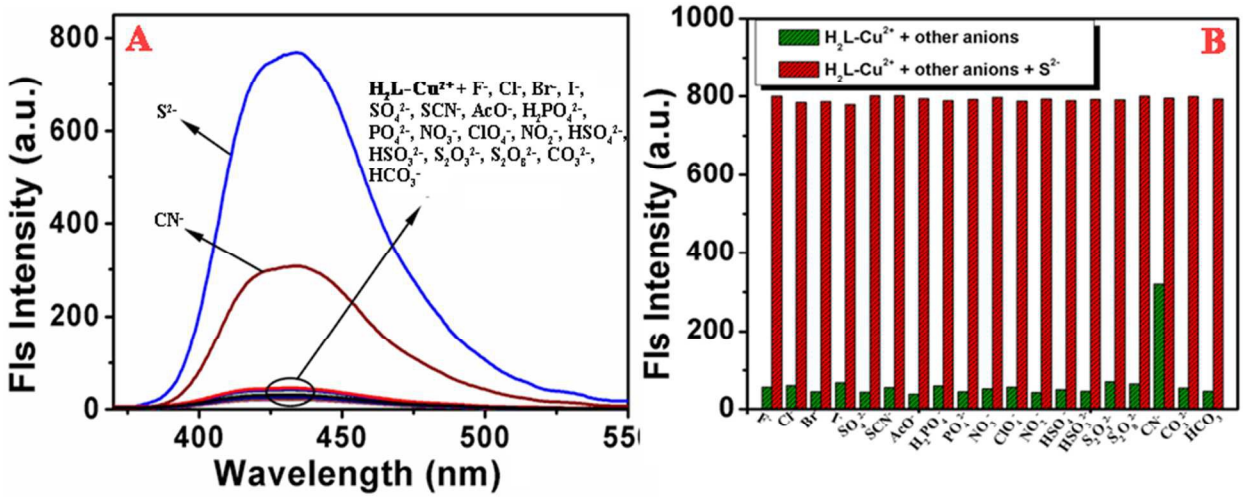

Fig. 10. (A) Change in the initial fluorescence intensities at λ = 425 nm (λ_{ex} = 365 nm) of **H_2L-Cu^{2+}** (5 μM) in the presence of 10 equiv. of different anions. (B) Competitive selective binding affinity of **H_2L-Cu^{2+}** (5 μM) in the presence of 10 equiv. of different anions in DMF/0.02 M HEPES (1:1, v/v, pH = 7.4) medium.

In addition, in order to investigate the "off-on" property induced by S^{2-}, the ESI-MS spectrum of the **H_2L-Cu^{2+}** with S^{2-} was run. The molecular ion peak observed at m/z 328.53 (calcd. 328.34) (Fig. S19, ESI) is assigned to [**H_3L** - H]$^-$, further elucidating the mechanism of sensing of sulfide anions by decomplexation and revival of the chemosensor.

Bioimaging studies

The interesting photophysical properties of **H_3L** for high selectivity, sensitivity and rapid-response towards Cu^{2+} and subsequent recognition for S^{2-} have further prompted us to extend our study to detect the Cu^{2+} and S^{2-} ions in biological systems by live cell imaging experiments. The DL cancer cells incubated for 1 h at 37 °C with **H_3L** (5 μM) showed considerable fluorescence due to the accumulation of **H_3L** within the cells [Fig. 11(A)]. However, in contrast, the staining of the pre-incubated cells with Cu^{2+} (5 μM) for 0.5 h at 37 °C exhibited almost no fluorescence [Fig. 11(D)], and the subsequent addition of S^{2-} (5 and 10 μM, respectively) regenerated the initial emission intensity of **H_3L** [Figs. 11(G) and 11(J)]. This result implies that the chemosensor **H_3L** is reversible and highly cellmembrane-permeable, and thus **H_3L** can be used as a biosensor to probe the intracellular Cu^{2+} and S^{2-} concentrations and investigate their bioactivity in living cells.

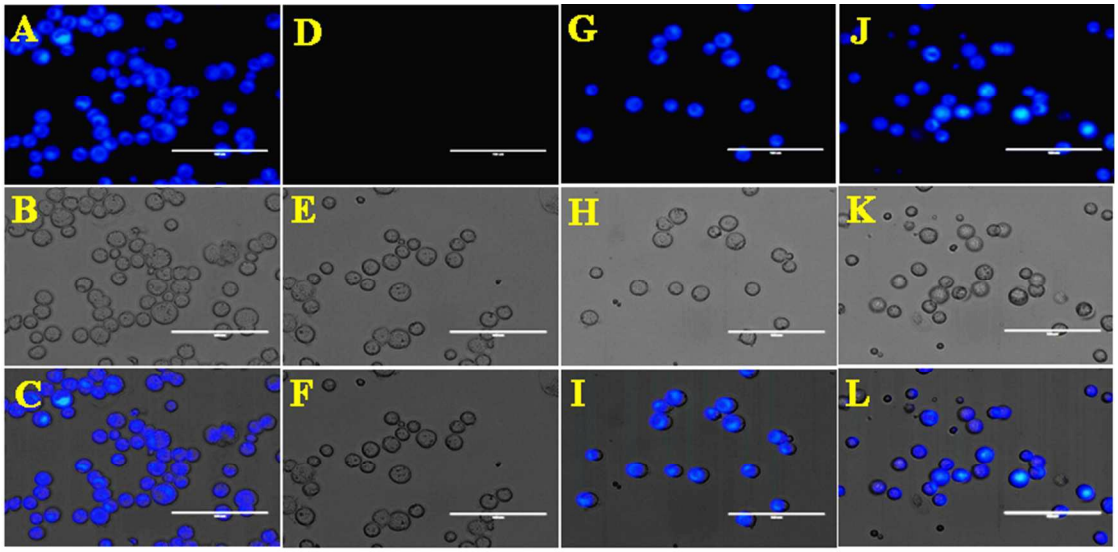

Fig. 11. Fluorescence images of $\mathbf{H_3L}$, Cu^{2+} and S^{2-} in DL cells. (A) Cells loaded with $\mathbf{H_3L}$ (5 μM) probe (B) Phase contrast image of A. (C) Overlay of A and B. (D) Cells incubated with $\mathbf{H_3L}$ (5 μM) and Cu^{2+} (5 μM) for 0.5 h. (E) Phase contrast image of D. (F) Overlay of D and E. (G) Cells treated with S^{2-} (5 μM) to $\mathbf{H_2L}$ + Cu^{2+} (5 μM) for 0.5 h. (H) Phase contrast images of G. (I) Overlay images of G and H. (J) Cells treated with S^{2-} (10 μM) to $\mathbf{H_2L}$ + Cu^{2+} (5 μM) for 0.5 h. (K) Phase contrast images of J. (L) Overlay images of J and K.

Besides, the cell viability of $\mathbf{H_3L}$ and $\mathbf{H_2L\text{-}Cu^{2+}}$ was evaluated using MTT assay (Fig. S19, ESI) with $\mathbf{H_3L}$ and $\mathbf{H_2L\text{-}Cu^{2+}}$ over a range of concentrations for 24 h. The IC_{50} values of compounds ($\mathbf{H_3L}$, 75 μM and $\mathbf{H_2L\text{-}Cu^{2+}}$, 100 μM) under investigation revealed that they do not negatively affect the cell viability over the full range of concentrations measured, indicating that they exhibit no serious cytotoxicity and could reasonably be used for intracellular detection. Therefore, the chemsensor $\mathbf{H_3L}$ could be useful for detecting Cu^{2+} and sequential detection of S^{2-} in biological systems.

Conclusions

This work concerns the synthesis and characterization of a new quinazoline functionalized benzimidazole-based fluorogenic chemosensor **H_3L** for selective and sensitive detection of Cu^{2+} ion and sequential recognition of S^{2-} ion by the derived **H_2L-Cu^{2+}** complex. In addition, it demonstrates that this new chemosensor can be utilized in live cell imaging of Cu^{2+} and S^{2-} ions respectively. The excellent detection limits of **H_3L** for Cu^{2+} (1.6×10^{-9} M) and **H_2L-Cu^{2+}** for S^{2-} (5.2×10^{-6} M) can be useful in the detection of trace amounts of Cu^{2+} and S^{2-} ions in biological and ecological samples.

Acknowledgments

This work has been partially supported by the Fundação para a Ciência e a Tecnologia (FCT), Portugal, and its UID/QUI/00100/2013 program. The authors A.P. and S.A. are grateful to the FCT for the award of a postdoctoral fellowship (ref: SFRH/BPD/88450/2012 and SFRH/BPD/76451/2011). The authors also acknowledge the Portuguese NMR Network (IST-UL Centre) for access to the NMR facility, and the IST Node of the Portuguese Network of mass-spectrometry (Dr. Conceição Oliveira) for the ESI-MS measurements.

Supporting Information

Electronic Supplementary Information (ESI) available: CCDC deposition No. CCDC 1059270, NMR, ESI MS spectral data of the compounds and sensor study plots.

References

1 B. Valeur and I. Leray, *Coord. Chem. Rev*., 2000, **205**, 3.

2 P. A. Gale, *Coord. Chem. Rev*., 2003, **240**, 19.

3 K. L. Haas and K. Franz, *J. Chem. Rev*., 2009, **109**, 4921.

4 A. Okamoto, T. Ichiba and I. Saito, *J. Am. Chem. Soc.,* 2004, **126**, 8364.

5 G. M. Gadd, *Microbiology*, 2010, **156**, 609.

6 K. M. K. Swamy, S. K. Ko, S. K. Kwon, H. N. Lee, C. Mao, J. M. Kim, K. H. Lee, J. Kim, I. Shin and J. Yoon, *Chem. Commun.,* 2008, **45**, 5915.

7 E. Gaggelli, H. Kozlowski, D. Valensin and G. Valensin, *Chem. Rev.*, 2006, **106**, 1995.

8 B. P. Zietz, J. Dassel de Vergara and H. Dunkelberg, *Environ. Res.,* 2003, **92**, 129.

9 (a) H. S. Seleem, G. A. El-Inany, B. A. El-Shetary and M. A. Mousa, *J. Chem. Cent.*, 2011, **5**, 20; (b) H. S. Seleem, G. A. El-Inany, B. A. El-Shetary and M. A. Mousa, *J. Chem. Cent.*, 2011, **5**, 20; (c) M. Shalash, A. Salhin, T. T. Theng, M. I. Saleh and B. Saad, *J. World Appl. Sci.*, 2011, **15**, 599; (d) P. Xie, F. Guo, C. Li and Y. Xiao, *Can. J. Chem.*, 2011, **89**, 1364; (e) G. He, Y. Zhao, C. He, Y. Liu and C. Duan, *Inorg. Chem.*, 2008, **47**, 5169; (f) Y. Xiang, A. Tong, P. Jin and Y. Ju, *Org. Lett.*, 2006, **8**, 2863.

10 (a) Q. Guo, C. Zhong, Y. Lu, C. Shi and Z. Li, *J. Inclusion Phenom. Macrocyclic Chem*., 2012, **72**, 79; (b) A. S. M. Ali, N. A. Razak and I. A. B Rahman, *The Scientific World Journal*, 2012, 1-10; (c) T. Li, Z. Yang,Y. Li, Z. Liu, G. Qi and B. Wang, *Dyes Pigm.*, 2011, **88**, 103; (d) E. E. Bellido, M. D. G. Riano, M. G. A-Vargas and R. Narayanaswamy, *Appl. Spectrosc.*, 2010, **64**, 727; (e) X. Chen, M. J. Jou, H. Lee, S. Kou, J. Lim, S. W. Nam, S. Park, K. M. Kim and J. Yoon, *Sens. Actuators*, B, 2009, **137**, 597.

11 (a) B. P. Zietz, H. H. Dieter, M. Lakomek, H. Schneider, B. Kessler-Gaedtke and H. Dunkelberg, *Sci. Total Environ.*, 2003, **302**, 127; (b) B. Schleper and H. J. Stuerenburg, *J. Neurol*., 2001, **248**, 705; (c) G. Georgopoulos, A. Roy, M. J. Yonone-Lioy, R. E. Opiekun and P. J. Lioy, *J. Toxicol. Health, Part B*, 2001, **4**, 341. (d) R. Uauy, M. Olivares and M. Gonzalez, *Am. J. Clin. Nutr.*, 1998, **67**, 952.

12 International Programme on Chemical Safety, Hydrogen Sulphide, World Health Organization, Geneva, Environmental Health Criteria, 19, 1981.

13 C.´ Szabo, *Nat. Rev. Drug Discovery*, 2007, **6**, 917.

14 (a) X. Cao, W. Lin, L. He, *Org. Lett.*, 2011, **13**, 4716; (b) P. Patnaik, A Comprehensive Guide to the Hazardous Properties of Chemical Substances, 3rd ed.; Wiley: New York, 2007; (c) S. A. Patwardhan, S. M. Abhyankar, Toxic and hazardous gases. IV, Colourage, 1988, **35**, 15.

15 (a) X. F. Yang, L. P. Wang, H. M. Xu, M. L. Zhao, *Anal. Chim. Acta*, 2009, **631**, 91; (b) M. Colon, J. L. Todoli, M. Hidalgo, M. Iglesias, *Anal. Chim. Acta*, 2008, **609**, 160; (c) R. F. Huang, X. W. Zheng, Y. Qu, *J. Anal. Chim. Acta*, 2007, **582**, 267; (d) F. Maya, J. M. Estela, V. Cerda,` *Anal. Chim. Acta*, 2007, **601**, 87; (e) Y. Jin, H. Wu, Y. Tian, L. H. Chen, J. J. Cheng, S. P. Bi, *Anal. Chem.*, 2007, **79**, 7176; (f) N. S. Lawrence, R. P. Deo, *J. Anal. Chim. Acta*, 2004, **17**, 131; (g) C. Giuriati, S. Cavalli, A. Gorni, D. Badocco, P. Pastore, *J. Chromatogr. A*, 2004, **1023**, 105; (h) D.´Jimenez, R. Martínez-Manez, F. Sancenon, J. V. Ros-Lis, A. Benito, J.´ Soto, *J. Am. Chem. Soc.*, 2003, **125**, 9000; (i) A. Safavi, M. A. Karimi, *Talanta*, 2002, **57**, 491; (j) J. X. Du, Y. H. Li, J. R. Lu, *Anal. Chim. Acta*, 2001, **448**, 79; (k) E. A. Guenther, K. S. Johnson, K. H. Coale, *Anal. Chem.*, 2001, **73**, 3481; (l) N. S. Lawrence, J. Davis, R. G. Compton, *Talanta*, 2000, **52**, 771; (m) S.

Balasubramanian, V. Pugalenthi, *Water Res.,* 2000, **34**, 4201; (n) Z. Pawlak, A. S. Pawlak, *Talanta*, 1999, **48**, 347; (o) M. F. Choi, P. Hawkins, *Anal. Chim. Acta*, 1997, **344**, 105; (p) H. D. Axelrod, J. H. Cary, J. E. Bonelli, J. P. Lodge, *J. Anal. Chem.*, 1969, **41**, 1856; (q) M. A. Spaziani, J. L. Davis, M. Tinani, M. K. Carroll, *Analyst*, 1997, **122**, 1555 ; (r) F. Pouly, E. Touraud, J. F. Buisson, O. Thomas, *Talanta* 1999, **50**, 737.

16 (a) F. J. Lebeda and S. S. Deshpande, *Anal. Biochem.*, 1990, **187**, 302-309; (b) J. Ma and P. K. Dasgupta, *Anal. Chim. Acta*, 2010, **673**, 117.

17 (a) Q. Meng,Y. Shi, C. Wang, H. Jia, X. Gao, R. Zhang, Y. Wanga and Z. Zhang, *Org. Biomol. Chem.*, 2015, **13**, 2918; (b) X. Qu, C. Li, H. Chen, J. Mack, Z. Guo and Z. Shen, *Chem. Commun.*, 2013, **49**, 7510; (c) C. Kar, M. D. Adhikari, A. Ramesh and G. Das, *Inorg. Chem.*, 2013, **52**, 743; (d) F. Hou, L. Huang, P. Xi, J. Cheng, X. Zhao, G. Xie, Y. Shi, F. Cheng, X. Yao, D. Bai, and Z. Zeng, *Inorg. Chem.,* 2012, **51**, 2454; (e) M. Q. Wang, K. Li, J. T. Hou, M. Y. Wu, Z. Huang and X. Q. Yu, J. *Org. Chem.*, 2012, 77, 8350; (f) K. Sasakura, K. Hanaoka, N. Shibuya, Y. Mikami, Y. Kimura, T. Komatsu, T. Ueno, T. Terai, H. Kimura, and T. Nagano, *J. Am. Chem. Soc.,* 2011, **133**, 18003.

18 (b) E. J. O'Neil and B. D. Smith, *Coord. Chem. Rev.*, 2006, **250**, 3068; (a) R. Martinez-Mãnez and F. Sancenon, *Chem. Rev.*, 2003, **103**, 4419.

19 (a) J. Chen, Y. Li, W. Zhong, Q. Hou, H. Wang, X. Sun and P. Yi, *Sens. Actuators, B*, 2015, **206**, 230; (b) Q. Zhou, Y. Zhu, P. Sheng, Z. Wu and Q. Cai, *RSC Adv.*, 2014, **4**, 46951; (c) C. Gao, X. Liu, X. Jin, J. Wu, Y. Xie, W. Liu, X. Yao and Y. Tang, *Sens. Actuators, B,* 2013, **185**, 125; (d) F. Hou, J. Cheng, P. Xi, F. Chen, L. Huang, G. Xie, Y. Shi, H. Liu, D. Bai and Z. Zeng, *Dalton Trans.*, 2012, **41**, 5799; (e) S. Rochat and K.

Severin, *Chem. Commun.*, 2011, **47**, 4391; (f) J. S. Wu, R. L. Sheng, W. M. Liu, P. F. Wang, J. J. Ma, H. Y. Zhang and X. Q. Zhuang, *Inorg. Chem.*, 2011, **50**, 6543; (g) L. Zhang, X. Lou, Y. Yu, J. Qin and Z. Li, *Macromolecules*, 2011, **44**, 5186; (h) D. P. Pluth, M. R. Chan, L. E. McQuade and S. J. Lippard, *Inorg. Chem.*, 2011, **50**, 9385; (i) X. D. Lou, J. G. Qin and Z. Li, *Analyst*, 2009, **134**, 2071.

20 (a) A. Kumar Mahapatra, S. Mondal, S. K. Manna, K. Maiti, R. Maji, Md. R. Uddin, S. Mandal, D. Sarkar, T. K. Mondal and Dilip Kumar Maitid, *Dalton Trans.*, 2015, **44**, 6490.

21 (a) M. Sun, H. Yu, H. Li, H. Xu, D. Huang, and S. Wang, *Inorg. Chem.,* 2015, **54**, 3766; (b) Y. Fu, Q. C. Feng, X. J. Jiang, H. Xu, M. Lia and S. Q. Zang, *Dalton Trans.*, 2014, **43**, 5815; (c) L. Tang, P. Zhou, Q. Zhang, Z. Huang, J. Zhao, M. Cai, *Inorg. Chem. Comm.*, 2013, 36, 100; (d) Y. B. Ruan, A. F. Li, J. S. Zhao, J. S. Shen and Y. B. Jiang, *Chem. Commun.*, 2010, **46**, 4938.

22 D. D. Perrin, W. L. F. Armango and D. R. Perrin, *Purification of Laboratory Chemicals*; Pergamon: Oxford, U.K. 1986.

23 (a) Bruker, APEX2 & SAINT, AXS Inc., Madison, WI, **2004**; (b) G. M. Sheldrick, *Acta Cryst*., 2008, **A64**, 112; (c) L. J. Farrugia*, J. Appl. Cryst.*, 1999, **32**, 837. (d) A. L. Spek, *Acta Cryst.*, 1990, **A46**, C34.

24 a) Y. Zhao and D. G. Truhlar, *Theor. Chem. Acc.,* 2008**, 120**, 215; (b) M. J. Frisch, G. W. Trucks, H. B. Schlegel, G. E. Scuseria, M. A. Robb, J. R. Cheeseman, G. Scalmani, V. Barone, B. Mennucci, G. A. Petersson, H. Nakatsuji, M. Caricato, X. Li, H. P. Hratchian, A. F. Izmaylov, J. Bloino, G. Zheng, J. L. Sonnenberg, M. Hada, M. Ehara, K. Toyota, R. Fukuda, J. Hasegawa, M. Ishida, T. Nakajima, Y. Honda, O. Kitao, H. Nakai, T. Vreven,

Jr., J. A. Montgomery, J. E. Peralta, F. Ogliaro, M. Bearpark, J. J. Heyd, E. Brothers, K. N.Kudin, V. N. Staroverov, R. Kobayashi, J. Normand, K. Raghavachari, A. Rendell, J. C. Burant, S. S. Iyengar, J. Tomasi, M. Cossi, N. Rega, J. M. Millam, M. Klene, J. E. Knox, J. B. Cross, V. Bakken, C. Adamo, J. Jaramillo, R. Gomperts, R. E. Stratmann, O. Yazyev, A.J. Austin, R. Cammi, C. Pomelli, J. W. Ochterski, R. L. Martin, K. Morokuma, V. G.Zakrzewski, G. A. Voth, P. Salvador, J. J. Dannenberg, S. Dapprich, A. D. Daniels, O. Farkas, J. B. Foresman, J. V. Ortiz, J. Cioslowski and D. J. Fox, Gaussian 09, Revision A.01, Gaussian, Inc., Wallingford CT, 2009.

25 M. Dolg, U. Wedig, H. Stoll and Preuss, H., *J. Chem. Phys.,* 1987, **86**, 866.

26 (a) J. Tomasi and M. Persico, *Chem. Rev.,* 1994, **94**, 2027; (b) V. Barone and M. Cossi, *J. Phys. Chem. A.,* 1998, **102**, 1995.

27 D. H. Wertz, *J. Am. Chem. Soc.,* 1980, **102**, 5316.

28 J. Cooper and T. Ziegler, *Inorg. Chem.,* 2002, **41**, 6614.

29 T. J. Mosmann, *J. Immunol. Methods,* 1983. **65**, 55.

30 H. Karabiyik, O. Erdem and M. Aygun, *J. Inorg. Organomet. Polym.,* 2010, **20**, 142; (c) L. Mouni, M. Akkurt and S.O. Yildirm, *J. Chem. Crystallogr.,* 2010, **40**, 169; (b) P. Mukherjee, M.G.B. Drew and A. Figuerola, *Polyhedron,* 2008, **27**, 3343.

31 L. Tang, M. Cai, Z. Huang, K. Zhong, S. Hou, Y. Bian and R. Nandhakumar, *Sens. Actuators, B*, 2013, **185**, 188.

32 (a) Y. Thio, X. Yang and J. J. Vittal, *Dalton Trans*., 2014, **43**, 3545. (b) S. Anbu, M. Kandaswamy, S. Kamalraj, J. Muthumarry and B. Varghes, *Dalton Trans*., 2011, **40**, 7310.

33 (a) S. Anbu, R. Ravishankaran, M. F. C. Guedes da Silva, A. A. Karande and A. J. L. Pombeiro, *Inorg. Chem.*, 2014, **53**, 6655; (b) S. Anbu, S. Shanmugaraju, R. Ravishankaran, A. A. Karande and P. S. Mukherjee, *Inorg. Chem. Commun.*, 2012, **25**, 26; (c) Z. Li, L. Zhang, L. Wang, Y. Guo, L. Cai, M. Yu, L. Wei, *Chem. Commun.*, 2011, **47**, 5798; (d) H. S. Jung, P. S. Kwon, J. W. Lee, J. I. Kim, C. S. Hong, J. W. Kim, S. Yan, J. Y. Lee, J. H. Lee, T. Joo, J. S. Kim, *J. Am. Chem. Soc.,* 2009, **131**, 2008.

34 (a) L. Huang, F. Chen, P. Xi, G. Xie, Z. Li, Y. Shi, M. Xu, H. Liu, Z. Maa, D. Bai and Z. Zeng, *Dyes and Pigments*, 2011, **90**, 265; (b) H. Qin, J. Ren, J. Wang and E. Wang, *Chem. Commun.,* 2010, **46**, 7385; (*c*) X. Y. Zhao, Y. Liu and K. S. Schanze, *Chem. Commun*., 2007, 2914; (d) M. Beltramello, M. Gatos, F. Mancin, P. Tecillab and U. Tonellatoa, *Tetrahedron Lett.,* 2001, **42**, 9143.

35 World Health Organization. Guidelines for drinking-water quality. 3. Geneva: 2008, 188.

Table 1 Crystal data and structure refinement parameters for **H_3L**

	H_3L
Empirical formula	$C_{46}H_{46}N_8O_7$
Crystal system	monoclinic
Space group	C 2/c
a (Å)	19.236(3)
b (Å)	17.580(3)
c (Å)	14.370(3)
β (deg)	126.193(4)
V (Å^3), *Z*	3921.7(12)
λ (Å)	0.71069
Colour and habit	bonze, block
T (K)	296(2)
reflns collected	37965
Refins obs / unique	3884 / 2934
D_{calcd} (Mg m^{-3})	1.394
μ (mm^{-1})	0.096
GOF on F^2	1.082
R_{int}	0.0545
final *R* indices $I>2\sigma(I)$	R1 = 0.0870
	wR2 = 0.2331
R indices (all data)	R1 = 0.1070
	0.2453